Seifert, R. A., Hart, C. E., Phillips, P. E., Forstrom, J. W., Ross, R., Murry, M. J., & Bowen-Pope, D. F. (1989) *J. Biol. Chem. 64*, 8771–8778.
Ueno, H., Colbert, H., Escobedo, J. A., & Williams, L. T. (1991) *Science 151*, 844–848.
Waterfield, M. D., Scrace, G. F., Whittle, N., Stroobant, P., Johnsson, A., Wasteson, A., Westermark, B., Heldin, C. H., Huang, J. S., & Deuel, T. F. (1983) *Nature (London) 304*, 35–39.
Williams, L. T. (1989) *Science 243*, 1564–1570.
Yarden, Y., Escobedo, J. A., Kuang, W. J., Yang-Feng, T. L., Daniel, T. O., Tremble, P. M., Chen, E. Y., Ando, M. E., Harkins, R. N., Francke, U., Fried, V. A., Ullrich, A., & Williams, L. T. (1986) *Nature (London) 323*, 226–232.

Distances between the Antigen-Binding Sites of Three Murine Antibody Subclasses Measured Using Neutron and X-ray Scattering†

T. R. Sosnick, D. C. Benjamin,‡ J. Novotny,§ P. A. Seeger, and J. Trewhella*

Life Sciences Division and LANSCE, Los Alamos National Laboratory, Los Alamos, New Mexico 87545, Department of Microbiology, University of Virginia, Charlottesville, Virginia 22908, and Department of Macromolecular Modeling, Bristol-Myers Squibb Research Institute, Princeton, New Jersey 08543

Received August 29, 1991; Revised Manuscript Received November 13, 1991

ABSTRACT: For three different murine immunoglobulins (IgG subclasses 1, 2a, and 2b), the distances between their antigen-binding sites have been measured using neutron scattering from deuterated antigens complexed with proteated IgG. Neutron-scattering data were measured for each antibody–antigen complex in a 41% D_2O solvent. Unlike the proteated antibody molecule, the deuterated antigens are strongly contrasted against the 41% D_2O solvent and give rise to a scattering profile that contains an interference term related to the distance between the deuterated antigens. For all three subclasses, the damping of this interference term, which gives information on the relative flexibility of the antigen-binding sites, indicates that a single distance is inadequate to describe the observed scattering and a distribution of distances is needed. The scattering profile has been modeled for each subclass to give the mean distance between the antigens and the variance of this distance. For all three IgG subclasses, the mean distance is between 117 and 134 Å, and the variance is large (≈40 Å), indicating a high degree of flexibility of the F_{ab} arms. Small-angle X-ray scattering measurements on the same samples are consistent with the neutron-scattering results.

Antibodies are protein products of the immune response which specifically recognize and bind to the foreign substance (antigen) which induced their synthesis. The antibody molecule is divided into two functional regions: the F_{ab} portion which contains the antigen-binding site and the non-antigen-binding F_c region. The totality of antigenic substances presents an almost infinite surface variability. Therefore, the immune system must be capable of responding by producing an almost limitless variety of antigen-binding sites. In contrast, a very limited number of classes and subclasses of antibody molecules have evolved, each of which is capable of performing one or more F_c region mediated biological functions such as the fixation of complement leading to lysis and/or phagocytosis of the offending foreign substance; interaction with F_c receptors on mast or phagocytic cells, leading to the release of pharmacologically active agents or phagocytosis, respectively; and transport across epithelial surfaces, including the intestine or the placenta providing maternal protection against infection.

Over 70% of the antibody in serum is of the IgG class. This class can be visualized as a "Y" or "T" shaped molecule having 2-fold symmetry with two identical antigen-binding sites, one at each end of two identical arms, or F_{ab} regions. The two F_{ab} regions are joined to an F_c region at a flexible hinge region (Noelken et al., 1965; Valentine & Green, 1967; Alpert et al., 1985; Reidler et al., 1982; Oi et al., 1984; Dangl et al., 1988). High-resolution crystallographic data exist on portions and fragments of IgG as well as hinge deleted IgG's [reviewed by Davies et al. (1990), Alzari et al. (1988), Davies and Metzger (1983), and Marquart and Deisenhofer (1982)]. However, information about the complete structure of functional IgG's is lacking. Detailed computer models of entire human IgG molecules incorporating the amino acid sequence of the hinge region of each subclass have been presented (Pumphrey, 1986), but there is little empirical evidence to support or refute these composite models. Small-angle X-ray and neutron solution scattering studies have been performed on human (Cser et al., 1976; Pilz et al., 1977; Kilar et al., 1985) and pig (Cser et al., 1978, 1981a) antibodies, but, due to the inherent problems of spherical averaging, it has not been possible to determine unique structures. Cser et al. (1978) used neutron solvent matching techniques to measure explicitly the distance between two antibody-bound antigens. The scattered neutron intensity from a molecule is proportional to the difference or contrast between the mean neutron-scattering length density of the molecule and that of the solvent. In the experiment of Cser et al. (1978), polyclonal pig serum IgG complexed with a

† This work was performed under the auspices of the DOE (Contract W-7405-ENG-36) and is supported by DOE/Office of Health and Environmental Research project KP-04-01-00-0 (J.T.) and National Institutes of Health Grant AI20745 (D.C.B.). This work has benefited from the use of facilities at the Manuel Lujan Jr. Neutron Scattering Center, a national user facility funded as such by DOE/Office of Basic Energy Sciences.

* Address correspondence to this author at Life Sciences Division, Los Alamos National Laboratory.
‡ University of Virginia.
§ Bristol-Myers Squibb Research Institute.

0006-2960/92/0431-1779$03.00/0

40-kDa dextran antigen was placed in 41% D_2O. The neutron-scattering density of the IgG molecule was thus matched to the solvent, and the scattering signal was primarily from the dextran antigens. The availability of monoclonal antibodies (mAb)[1] to monomeric antigens allows us to use similar methods to now study better defined systems. In particular, we can prepare large amounts of mAb's of different subclasses, each specific for the same antigen and sometimes the same site on that antigen. In addition, the existence of bacterial expression systems allows for the production of deuterated protein antigens which have much greater neutron contrast, and hence scattering signal, than dextran in 41% D_2O.

We report here the results of neutron and X-ray scattering measurements on murine mAb of the IgG1, IgG2a, and IgG2b subclasses. Using deuterated antigen and neutron contrast matching techniques, we have obtained a measure of the mean separation of the bound antigens as well as the variance of this distance which is a direct measure of the flexibility of the F_{ab} arms.

Materials and Methods

Sample Preparation. Monoclonal antibodies to the 16.8-kDa protein staphylococcal nuclease (NASE) [ribonucleate (deoxyribonucleate)-3′-nucleotidohydrolase, EC 3.1.4.7] were prepared as previously described (Smith et al., 1991). These antibodies bind NASE with association constants $K_A \approx 10^9$ M^{-1}. The specific monoclonal antibodies used were IgG1 (mAb 13), IgG2a (mAb 14), and IgG2b (mAb 23). Deuterated NASE was obtained using the λP9-NASE plasmid transformed into *Escherichia coli* strain AR120. The transformed cells were grown in 99%+ D_2O using 97%+ enriched deuterated algal hydrolizate (Celtone-D9 powder, Martek Corp., Columbia, MD). the λP9-NASE plasmid was obtained from David Shortle at John Hopkins University.

The IgG and NASE samples were combined at a 1:2 molar stoichiometry to a total protein concentration of 31 mg/mL in 41.5% D_2O with 45 mM phosphate buffer, pH 7.3, and 135 mM sodium chloride. At this high antigen concentration, 0.32 mM, both antibody-binding sites are occupied. Prior to mixing, the antibody samples were spun at 100000*g* for 12 min, and the final concentration was determined photometrically using an extinction coefficient of $\epsilon_{280}^{1\%} = 15$ for IgG. Similarly, the stock NASE samples were spun at 16000*g* for 5 min, and the concentration was determined using an extinction coefficient of $\epsilon_{280}^{1\%} = 9.3$. The samples were prepared using lyophilized proteins whose solvent-exchangable hydrogens were all initially proteated. A decrease in D_2O level from 41.5% to 41.0% upon addition of proteins to the buffer solution was calculated assuming all noncovalently bound hydrogens exchanged with the solvent. The neutron measurements were completed within 48 h of sample preparation. The samples were stored at 4 °C and X-ray measurements were performed within a week of the neutron measurements.

High-purity bovine serum albumin (Sigma Chemical Co., product number A-0281) was used as a protein standard for the X-ray experiments in order to estimate the molecular weight of the scattering particle and to check for protein aggregation. Albumin standards were prepared from lyophilized proteins dialyzed extensively against an H_2O solution with 50 mM phosphate buffer, pH 7.2, and 100 mM sodium chloride. Protein concentrations were determined photometrically ($\epsilon_{280}^{1\%} = 6.67$) and were 30–40 mg/mL.

Table I: Neutron-Scattering Length Densities[a]

component	neutron-scattering length density (cm^{-2})
H_2O	-0.56×10^{10}
D_2O	6.4×10^{10}
proteated IgG	2.3×10^{10}
deuterated NASE	7.3×10^{10}

[a] Scattering length densities were calculated as $\sum b_i/V$ where the b_i's are the neutron-scattering lengths for each atom in the molecule and V is the molecular volume. The calculated values for the proteins assume that the labile hydrogens have exchanged with a 41% D_2O solvent.

Small-Angle Neutron and X-ray Scattering. Small-angle neutron-scattering measurements were performed using the Low-Q Diffractometer (LQD) at the Manuel Lujan Jr. Neutron Scattering Center (LANSCE) at Los Alamos National Laboratory (Seeger et al., 1987, 1990). The neutron source is pulsed: a proton beam strikes a heavy metal target (e.g., tungsten), emitting a very short burst (≈20 μs) of neutrons having a wide range of wavelengths. At LQD, the energy of these neutrons is reduced significantly as they pass through a moderator, and neutrons having wavelengths in the range 0.2–15 Å are used. Because all the neutrons are emitted at essentially the same time, the wavelength λ of each neutron can be determined from the time of arrival at the two-dimensional detector. The scattered neutrons are recorded on a two-dimensional position-sensitive detector as a function of both time and scattering angle. Using the measured wavelength and scattering angle 2θ, the momentum transfer, or scattering vector Q, can be calculated using

$$Q = \frac{4\pi \sin \theta}{\lambda} \quad (1)$$

Importantly, the large wavelength distribution available enables LQD to measure a wide range of Q values at a single detector position. The reduced data are presented as dimensionless scattering probabilities, $(N/A)\, d\Sigma(Q)/d\Omega$, where N/A is the number of scattering particles per unit area of sample and $d\Sigma(Q)/d\Omega$ is the differential coherent scattering cross section per scatterer. Division of this quantity by the sample thickness gives the neutron intensity: $I(Q) = (N/V)\, d\Sigma(Q)/d\Omega$ in units of cm^{-1}, where N/V is the number of scattering particles per unit volume. The samples were measured in rectangular quartz cuvettes having a 1-mm path length. The beam size at the sample position was approximately 9 × 13 mm, and the sample was large enough to completely fill this area. Neutron data were collected on each subclass for approximately 28 h at an average proton beam current of 75 μA.

The X-ray scattering data were collected on the small-angle scattering spectrometer described in Trewhella et al. (1988). This station uses a line focus from a sealed-tube X-ray source powered by a generator operated at 1.2 kW. The X-rays are focused, using a quartz mirror, onto a lead beam stop mounted directly in front of a one-dimensional position-sensitive detector. The sample-to-detector distance was 64 cm, and the measurements were conducted at room temperature. Data acquisition times were approximately 12 h per measurement.

Neutron Contrast Matching Technique. The distances between the antigen-binding sites were measured using neutron contrast matching techniques as was done in Cser et al. (1978). The labeling of the proteins was accomplished by deuteration,

[1] Abbreviations: b, neutron-scattering length; c, protein concentration; D_c, mean antigen separation distance; d_{max}, maximum distance; $I(Q)$, scattering intensity per solid angle; mAb, monoclonal antibody; MW, molecular weight; NASE, staphylococcal nuclease; $P(r)$, pair-distance distribution function; prob(D), probability distribution of the antigen separation distance; Q, momentum transfer; R_g, radius of gyration; λ, neutron wavelength; σ, standard deviation; $\epsilon_{280}^{1\%}$, extinction coefficient for a 1% solution at 280 nm.

which takes advantage of the large difference between the neutron-scattering length of hydrogen and deuterium. The neutron-scattering intensity for a particle in a homogeneous solvent is proportional to the contrast factor $(\rho_p - \rho_s)^2$, where ρ_p is the mean neutron-scattering length density of the particle and ρ_s is the mean scattering length density of the solvent. Table I lists the average neutron-scattering length densities calculated for the different components of the measured samples. The neutron measurements were performed on proteated antibody complexed with two deuterated monovalent antigens in 41% D_2O solvent. The 41% D_2O solvent has the same mean neutron-scattering density as the proteated antibody molecule (Cser et al., 1976), and hence the antibody contributes negligibly to the scattering signal. However, the deuterated antigens are strongly contrasted against the 41% D_2O solvent. This gives rise to a spherically averaged scattering profile that contains an interference term related to the distance D between the deuterated globular antigens:

$$I(Q) = I_{NASE}(Q)\left[1 + \frac{\sin(QD)}{(QD)}\right] \quad (2)$$

where $I_{NASE}(Q)$ is the scattering from a single NASE, approximated as a centrosymmetric particle (Porod, 1982). The oscillations in this diffraction pattern are analogous to the oscillations in the well-known diffraction pattern from two slits.

Antibody complexed with proteated NASE also has very low contrast and is used to subtract, to first order, any contribution to the scattering signal due to density fluctuations within the IgG molecule or any potential mismatch of the 41% D_2O solvent to the proteated antibody.

Data Analysis. Data were reduced and analyzed as described in Heidorn et al. (1989). Structural parameters were derived using either Guinier or $P(r)$ analyses. The Guinier Approximation (Guinier, 1939), valid at very low Q, is

$$I(Q) = I(0)e^{-Q^2R_g^2/3} \quad (3)$$

where R_g is the radius of gyration of the particle and is defined as

$$R_g^2 = \int_V [\rho_p(r) - \rho_s] r^2 \, dV / \int_V [\rho_p(r) - \rho_s] \, dV \quad (4)$$

$\rho_p(r)$ is the scattering density of the particle, ρ_s is the mean scattering density of the solvent, and V is the particle volume. The density relevant for neutron scattering is the neutron-scattering length density $\Sigma b_i/V$, whereas the density relevant for X-ray scattering is the electron density. Unlike neutron-scattering length density, the X-ray scattering density of a deuterated protein is essentially identical to that of proteated protein.

The pair–distance distribution function $P(r)$ was calculated according to

$$P(r) = 1/2\pi^2 \int I(Q) Qr \sin(Qr) \, dQ \quad (5)$$

using the indirect Fourier transform method with slit-smearing developed by Moore (1980). The pair–distance distribution function is the frequency of vectors, connecting small-volume elements within the entire volume of the scattering particle, weighted by the product of the excess scattering densities in each volume element $(\rho_p - \rho_s)$.

For the X-ray scattering data, the effects of interparticle interference were corrected by a linear least-squares extrapolation to zero protein concentration of the experimental scattering functions divided by the protein concentration, $I(Q)/c$. The extrapolated scattering function was used to calculate the $P(r)$ function at infinite dilution.

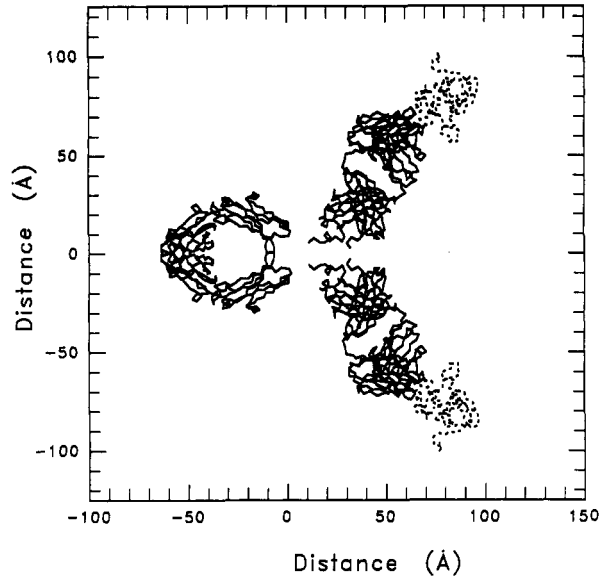

FIGURE 1: Composite model of the α-carbon backbone created from the crystal structure coordinates of the KOL F_{ab} subunit (Marquart et al., 1980) attached to the F_c subunit (Deisenhofer, 1981) of IgG (solid). The two NASE molecules (dash) (Cotton et al., 1979) are located at the antigen-binding sites at the tips of the F_{ab} subunits.

Model Calculations. The scattering and pair–distribution functions were calculated from models using two different methods. The first modeling procedure used with the neutron-scattering data assumes that the proteated antibody molecule is completely contrast matched so that the scattering signal is entirely due to the deuterated antigens. The antigens are approximated as spheres that best fit the NASE crystal structure (Cotton et al., 1979), and antibody flexibility is included by allowing the spheres to be located a variable distance apart. This distance is parameterized by a probability distribution, prob(D), of finding the antigens a distance D apart. The scattering from this model is

$$I(Q) = I_R(Q)\left[1 + \int \text{prob}(D)\frac{\sin(QD)}{(QD)} \, dD\right] + C \quad (6)$$

where C is a constant used to account for incoherent scattering of hydrogen and

$$I_R(Q) = I_R(0)\left[\frac{\sin(QR) - QR\cos(QR)}{(QR)^6}\right]^2 \quad (7)$$

is the scattering from a single sphere of radius R representing the deuterated antigen. A Gaussian parameterization of prob(D) with unity normalization is used:

$$\text{prob}(D) = 1/[(2\pi)^{1/2}\sigma] \exp[-(D - D_c)^2/2\sigma^2] \quad (8)$$

where D_c is the mean distance and σ is the standard deviation. The model $I(Q)$ was fit to scattering data using a least-squares procedure by varying R, D_c, σ, C, and an over-all scale factor. This model $I(Q)$ has been broadened by instrumental resolution (Hjelm, 1988). The pair–distribution function $P(r)$ is calculated from the model $I(Q)$ according to eq 5.

In order to quantitate the possible effects of contrast mismatch and internal density fluctuations, a second modeling procedure was used. This is a Monte Carlo integration technique applied to a composite model of the fragments of the antibody molecule complexes to two NASE molecules (Figure 1) constructed using the crystal structures of an F_c region (Deisenhofer, 1981) and an F_{ab_2} portion (Marquart et al., 1980) complexed to two deuterated NASE molecules

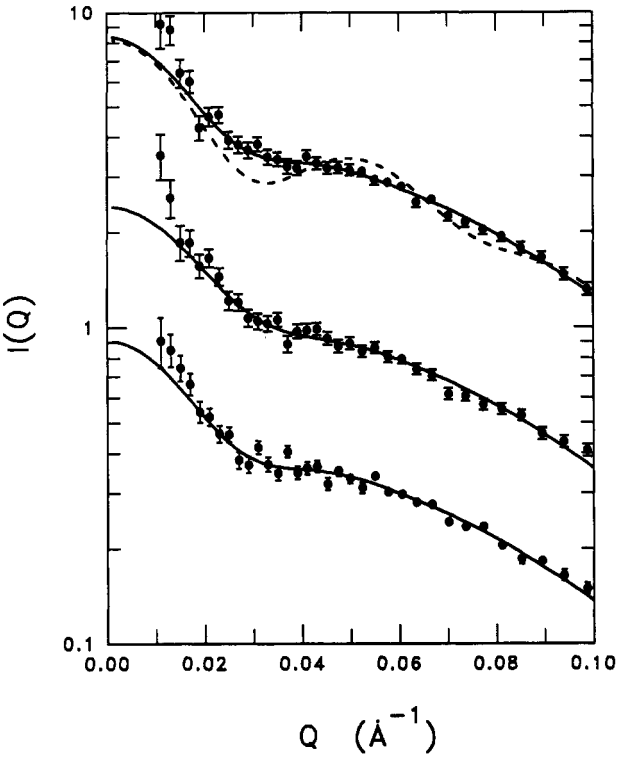

FIGURE 2: The background-subtracted neutron-scattering data with best fit (solid) of the flexible two-sphere model for IgG1 (top), IgG2a (middle), and IgG2b (bottom). For comparison, scattering from a rigid model described in text (dash) is also shown. Data are offset for readability.

(Cotton et al., 1979). Homogeneous spheres representing each amino acid are positioned at the α-carbon coordinates. The size and scattering power of each sphere was estimated from the volume and chemical composition of the represented amino acid. The pair–distribution function is calculated using a Monte Carlo procedure similar to that described in Heidorn and Trewhella (1988). The model structure is placed in a box, and a point is chosen randomly within the box. If the point is also contained within the model, it is saved. Distances between every pair of saved points are binned and weighted according to the product of the scattering powers at each point. The resulting histogram is the calculated $P(r)$ function. The scattering function $I(Q)$ is calculated from $P(r)$ according to the inverse of eq 5.

RESULTS

Neutron Scattering. The difference between the signal from IgG complexed with deuterated antigen and the background sample of proteated antigen and antibody for the three IgG subclasses is shown in Figure 2. The data from all three subclasses are similar, each showing a significant upturn at Q values below 0.025 Å^{-1}. Multiple oscillations which would result from the sin $(QD)/(QD)$ interference term are very weak or not discernible.

A model scattering profile was calculated for a rigid model comprised of the α-carbon coordinates of IgG derived from the protein crystal structures (see Materials and Methods) complexed to two deuterated NASE molecules represented by two spheres (Figure 1). Instrumental resolution (Hjelm, 1988) was included, but this did not change the results appreciably. Since the antibody molecule is contrast matched to the solvent, details of the model antibody structure do not significantly affect the model scattering, and the scattering function depends on the separation distance of the strongly contrasted antigens. As seen in Figure 2, the scattering calculated for the rigid model is significantly different than the observed scattering. The higher order oscillations in the model scattering profile resulting from the single antigen separation distance are not present in the observed scattering.

Table II: Fitting Parameters for the Flexible Two-Sphere Model to Neutron-Scattering Data[a]

subclass	D_c (Å)	σ (Å)	χ^2
IgG1	134 ± 5	40 ± 3	0.9
IgG2a	117 ± 4	37 ± 2	1.4
IgG2b	133 ± 4	38 ± 2	1.4

[a] D_c is the mean antigen separation distance, and σ is its standard deviation.

Since a rigid model is inconsistent with observed data, the data were fit with a model in which the two spherical antigens are located a variable distance apart (see Materials and Methods). For a distribution of distances, the scattering will be the sum of slightly out of phase sin $(QR)/(QR)$ terms, and the oscillations will be damped. The scattering measurements of free NASE indicate that it can be well approximated by a sphere. The values obtained for the radii of the spheres representing the bound NASE antigens varied between 22 and 25 Å. These values are determined primarily by the scattering data at high Q values (>0.05 Å^{-1}) and agree well with the values determined from X-ray (21.5 Å) and neutron (23.5 Å) scattering data of free NASE in solution. They are slightly larger than the 19 Å one would expect on the basis of the crystal structure for NASE (Cotton et al., 1979). This may be in part due to the presence of phosphate ions bound to the surface of the positively charged NASE molecule. For consistency, all fits to the data were conducted using a fixed radius of 23.5 Å, but the differences between the resulting fitting parameters and those where the radii were allowed to vary were within statistical error. The resolution broadened fits to the $I(Q)$ data for the three antibodies are shown in Figure 2, and fitting parameters are listed in Table II.

For all the antibodies, the mean distances, D_c, between the antigen centers are very similar and lie between 117 and 134 Å with standard deviations, σ, between 37 and 40 Å (Table II). The σ values observed imply that the three antibody subclasses are all similarly very flexible and the antigens may sometimes even come into contact with each other. The pair–distribution functions $P(r)$ for the deuterated antigen complexed with solvent matched antibodies were calculated from the fitted model curves, and these are shown in Figure 3 along with the respective $P(r)$ functions calculated directly from the scattering data using the indirect Fourier transform method (Moore, 1980), which, unlike the flexible two-sphere model, does not include any specific assumptions concerning the nature of the scattering species. As a result, more adjustable parameters are needed to adequately fit the data. Even so, the $P(r)$ functions obtained using the indirect Fourier transform method are very similar to those obtained using the two-sphere model except for the oscillations seen in the broad peak at longer r values. These oscillations are artifacts attributable in part to truncation effects due to the fact that the transform is conducted only over the finite Q range that can be measured.

The $P(r)$ functions determined for all three subclasses are strikingly similar and have two distinct features. The first is a sharp peak centered at 25 Å having a width of 50 Å arising from vector distances within a single NASE molecule. An independent measurement of deuterated NASE in the absence of antibody, also in 41% D_2O, produced an identical peak, confirming this interpretation. The second feature in the $P(r)$ curve is the broad peak centered at approximately 130 Å. This

Table III: Structural Parameters Derived from X-ray Scattering, Extrapolated to Infinite Dilution

subclass	R_g[a] (Å)	R_g[b] (Å)	d_{max} (Å)	mass from $I(0)$[c] (kDa)	mass from sequence (kDa)
IgG1	55.4 ± 1.6	55.5 ± 1.0	175	159 ± 3	150
IgG1/antigen	59.9 ± 1.8	65.7 ● 1.2	205	196 ● 5	184
composite model	56		155		
model/antigen	65		195		

[a] From Guinier analysis over the Q range 0.017 Å^{-1} to $1.3/R_g$. [b] From $P(r)$ analysis over the Q range 0.017–0.15 Å^{-1}. [c] Calculated from $I(0)$ using bovine serum albumin as a mass standard.

peak includes only vectors between bound antigens on the same IgG. The $P(r)$ curves at the bottom of Figure 3 were calculated for the rigid model shown in Figure 1. Importantly, the rigid model gives a much sharper interantigen peak than is observed in the $P(r)$ functions derived from the scattering data. [Note: Care should be taken not to interpret $P(r)$ as prob(D), the latter being the probability of finding the centers of the antigens a distance D apart. Rather, $P(r)$ is the probability of finding a vector of length r going from one scattering center to an other. For example, vector distances r between two 50-Å diameter antigens located a fixed center-to-center distance, D, apart would be in the range $r = D \pm 50$ Å.]

The scattering from proteated NASE–IgG complex in 41% D_2O solvent minus a 41% D_2O blank was small and flat, confirming that the mean solvent scattering length density was quite close to the match point of the antibody. However, to evaluate potential contributions from even a slight contrast mismatch between the antibody and the 41% D_2O solvent, or from any internal neutron-scattering length density fluctuations within the antibody molecule, additional model calculations were performed. The composite crystallographic model in Figure 1 contains the essential features needed to demonstrate the strength of the antigen signal in relation to any signal due to antibody mismatch. Pair–distribution functions were calculated for solvent deuteration levels of 39%, 41%, and 43% D_2O (Figure 3). No appreciable intensity in $P(r)$ was found in the region between 50 and 100 Å, and the function is dominated by the two features arising from intra- and inter-antigen vectors. Finally, the procedure of subtracting the completely proteated NASE–IgG sample minimizes the potential effects of any contrast mismatch of the antibody molecule. It can therefore be concluded that the observed signal is dominated by scattering from the two deuterated antigens.

Another concern in interpreting the scattering data is possible sample aggregation resulting in the measurement of distances between antigens on different antibodies. This was checked by performing small-angle X-ray scattering on the antibody–antigen complexes after the neutron measurements. Only a small amount of aggregation was observed (see below), which might be the cause of the neutron data points being slightly higher than the model fit at very low Q. However, this did not interfere with interpretation of the data because the higher Q data are more important in determining the model parameters.

X-ray Scattering. X-ray scattering data were collected on antibodies with and without antigen at protein concentrations ranging from 5 to 40 mg/mL. Unlike the procedure used for the neutron-scattering subtraction, the X-ray background blank is only solvent and the resulting scattering signal is from the equally contrasted antibody and antigen. As with neutron scattering, X-ray scattering measures a time-averaged structure.

The Guinier regions of the scattering curves extrapolated to infinite dilution are shown in Figure 4. Protein aggregation would be manifested by an upturn in the data above the linear

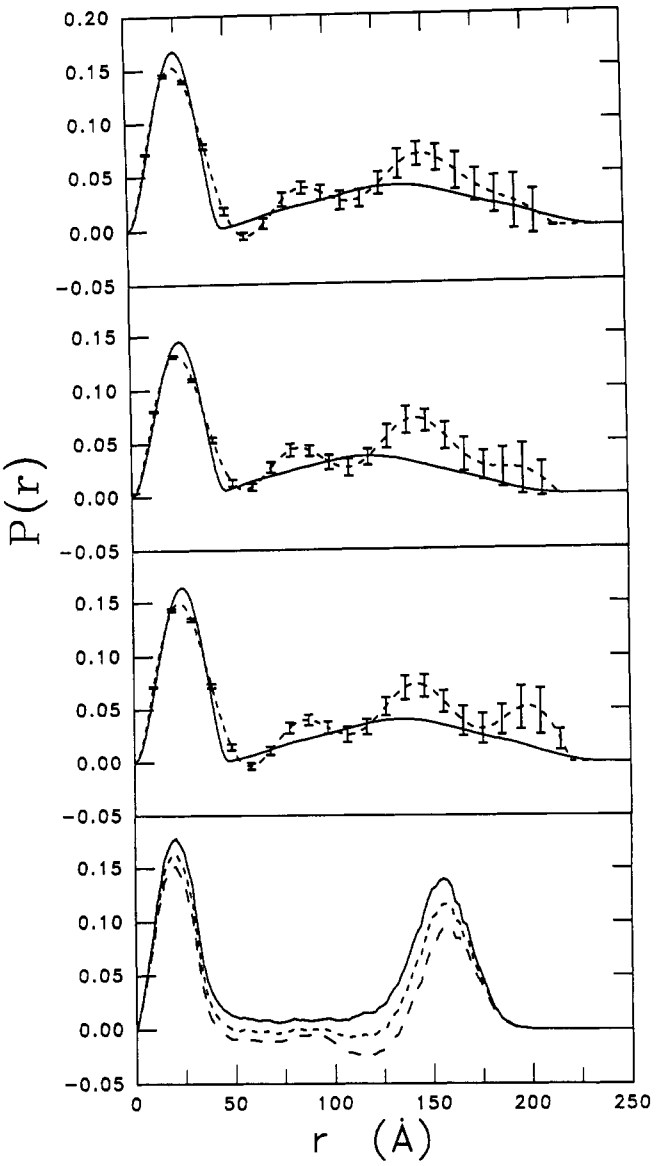

FIGURE 3: Pair–distance distribution function $P(r)$ obtained from the best fit $I(Q)$ to the neutron-scattering data for the flexible two-sphere model (solid) and for the Moore algorithm (short dash) for IgG1 (top), IgG2a (upper middle), and IgG2b (lower middle). For comparison, $P(r)$, calculated for the rigid composite IgG model attached to two spheres representing the deuterated antigens, is shown (bottom). These distribution functions are calculated for solvent deuteration levels of 39% (long dash), 41% (short dash), and 43% (solid) D_2O.

fits at the lowest Q values. For the subclass IgG1 with and without antigen, the degree of aggregation was minimal and there was a region over which a fit could be performed where the Guinier approximation was valid ($R_gQ \leq 1.3$). The results of the Guinier analysis for IgG1 with and without antigen are listed in Table III. An *upper limit* on the fraction of aggregates in the IgG1 sample was estimated at <6%, assuming no higher order aggregates than dimers, from the difference

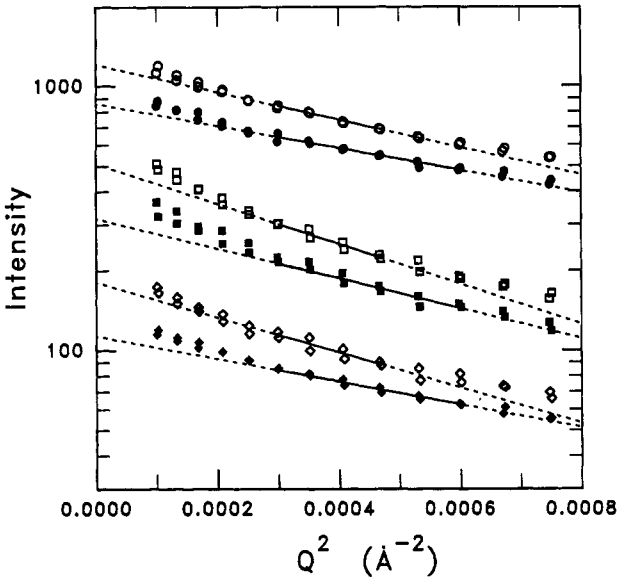

FIGURE 4: Guinier region of the X-ray scattering curves extrapolated to infinite dilution for antibody in the absence (filled) and presence (hollow) of antigen for IgG1 (circles), IgG2a (squares), and IgG2b (diamonds). Errors propagated from the counting statistics are smaller than the size of the symbols. The solid lines indicate the range over which the data were fit according to the Guinier approximation, and the short dashed lines are extrapolations of the fits. Data are offset for readability.

between the extrapolation of the Guinier fit and the value of the data at $Q = 0$ Å^{-1} (Hubbard et al., 1988). For both IgG2a and IgG2b with and without antigen, the amount aggregation was larger than observed for IgG1 and it precluded a rigorous Guinier analysis. Estimates of the degree of aggregation using the same approach as for IgG1 are approximately 18% and 7% for IgG2a and IgG2b with antigen, respectively. While a rigorous Guinier analysis using the appropriate Q region was not possible on IgG2a and IgG2b, a linear fit could be performed over the slightly more extended Q range 0.02–0.036 Å^{-1} ($R_gQ \leq 2.0$). For the unbound antibody, the calculated R_g was 54.3 ± 0.4 Å and 49.1 ± 0.3 Å for IgG2a and IgG2b, respectively. We stress that these values are potentially underestimates of the true values. For example, the value for R_g of IgG1 computed over this extended range was about 10 Å smaller than value computed over the valid Guinier range. No further analysis on these two subclasses was deemed appropriate.

The observed value of 56 Å or R_g of the murine subclass IgG1 is approximately 5–20 Å small than observed in previous small-angle scattering measurements from human and pig IgG [reviewed in Cser et al. (1981b)] with two exceptions. The first is the work by Kilar et al. (1985), who measured an R_g of 49 Å for human IgG3 over a Q range which extended out to 0.036 Å^{-1} ($R_gQ \leq 1.8$). The other exception is found in the work of Pilz et al. (1977), who calculated an R_g of 58 Å over the range $R_gQ \leq 1.5$ in the intact human IgG1 (KOL).

Pair–distance distribution functions, $P(r)$ (Figure 5), were calculated using the indirect Fourier transform method (Moore, 1980) for IgG1 with and without antigen from the X-ray scattering data extrapolated to infinite dilution over the Q range 0.017–0.15 Å^{-1}. The derived values for the R_g and the maximum dimension, d_{max}, are listed in Table III. The values for the R_g are slightly different than the values obtained by Guinier analysis because $P(r)$ analysis uses data over the entire Q range and does not assume the structure of interest is spherical. For these reasons, the $P(r)$ analysis is considered more accurate.

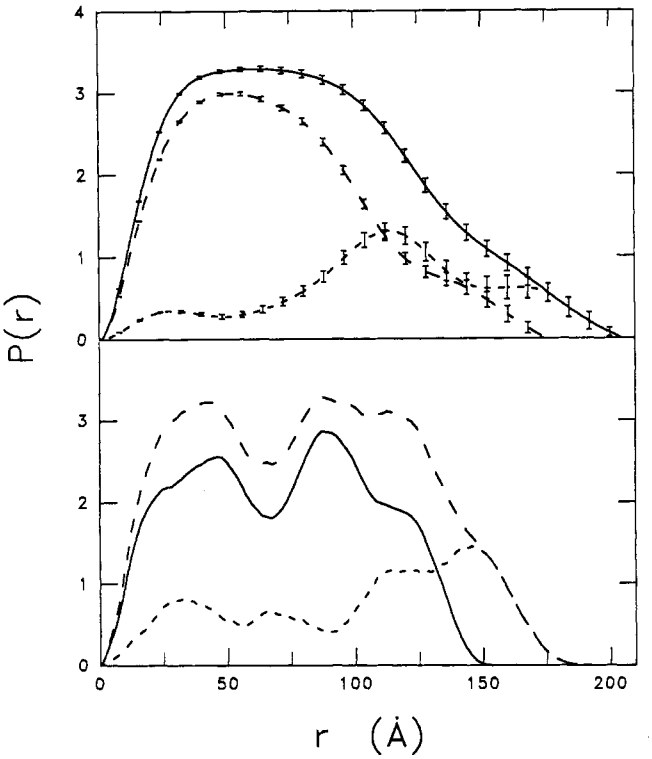

FIGURE 5: Pair–distance distribution function $P(r)$ calculated using the indirect Fourier transform method (Moore, 1980) and the X-ray scattering data extrapolated to infinite dilution for antibody in the presence (solid), absence of antigen (dash) and the difference between the two (short dash) for IgG1 (upper) and the rigid model described in text (lower).

The concentration dependence of $I(0)/c$ and R_g^2 for IgG1 with and without antigen (data not shown) shows no or only a slight decrease in both quantities with increasing concentration. This implies that dependence upon concentration is minimal, which is important because the neutron measurements were performed at the highest concentrations. The scattering data were put on a relative scale using bovine serum albumin as a mass standard (Kringbaum & Kugler, 1970) in order to estimate the molecular mass of the scattering species. The calculated molecular masses (Table III) for IgG1 with and without antigens were within experimental error of the known monomeric weights. This confirms that sample aggregation was minimal in these samples and the effects on the scattering were confined to the lowest Q values (<0.017 Å^{-1}) which could effectively be excluded from the data analysis.

The $P(r)$ function for subclass IgG1 without antigen peaks at 50 Å and has a maximum dimension, d_{max}, of 175 Å. As expected, the $P(r)$ function for the IgG1–antigen complexes has more long vectors. This is shown explicitly in the difference function which contains inter- and intraantigen vector distances along with vector distances between an antigen and the antibody molecule (Figure 5). While the difference function cannot be decomposed into the three individual contributions, the feature centered at 25 Å can be interpreted as principally intraantigen distances. Similarly, the feature centered at 180 Å is from vector distances between antigens and possibly between an antigen and the tip of the F_c domain. The remaining vectors are antibody–antigen and interantigen distances. The maximum distance of 205 Å between the antigens is in excellent agreement with the maximum distance derived from the neutron-scattering measurement.

The rigid antibody model shown in Figure 1 has approximately the same R_g as is determined from the X-ray scattering data. However, the $P(r)$ function for the IgG model is sig-

nificantly different from that calculated from the scattering data (Figure 5). The model $P(r)$ has two distinct features at 40 and 100 Å arising from intra- and interdomain vectors, respectively. The sharpness of these features is a result of the each F_{ab} and F_c domain being well separated from the other domains. The experimental $P(r)$ functions lack these sharp features associated with distinct F_{ab} and F_c domains. The experimental functions can be interpreted as resulting from a flexible molecule, where the sharp features have been broadened by antibody motions. In a flexible structure, the variable distances between the domains generates intermediate distance vectors, thereby smoothing out the sharp features in $P(r)$. Otherwise, the experimental and the rigid model $P(r)$ functions are quite similar except at longer vector distances. The maximum dimension observed is greater by about 20 Å and is likely due to antibody motions which place either the F_c or a F_{ab} domain more distant from the other F_{ab} domain than in the rigid model. The model has the F_c domain separated from the F_{ab_2} domains by a hinge length of approximately 30 Å, and this model has an R_g of 56 Å. For completeness, we point out that this model is planar and is in the most extended conformation possible so the time-averaged R_g of a flexible structure would be slightly smaller. The actual F_c to F_{ab} separation distance cannot be determined from the experimental R_g because the complete motions of the antibody are unknown.

Discussion

The experiments described here give a direct measure of the distance between the centers of two antigens bound to IgG's in solution. The inherent problems of spherical averaging in interpreting small-angle scattering have been overcome through the use of neutron contrast matching techniques. This greatly simplifies interpretation of the scattering data because it is primarily from the two bound antigens and is a function of their separation distance. For all three subclasses, IgG1, IgG2a, and IgG2b, a single distance is inadequate to describe the observed scattering, and a distribution of distances is needed indicating flexibility in the F_{ab} arms. Other experiments have indicated that the arms are flexible about the central hinge region. They include hydrodynamic (Noelken et al., 1965), electron microscopy (Valentine & Green, 1967), neutron spin-echo (Alpert et al., 1985), and nanosecond flourescence polarization measurements (Reidler et al., 1982; Oi et al., 1984; Dangl et al., 1988). The scattering data further indicate that all three subclasses have a similar degree of structural flexibility in spite of the fact that the portion of the hinge region between the F_{ab} subunit and the first disulfide forming cysteine residue, which might be expected to influence the flexibility of the F_{ab} arms, varies from 4 to 11 residues (Kabat et al., 1987).

The scattering data for each subclass give mean distances between 117 and 134 Å for antigens bound to a single IgG, and the variance of the distance is 37 Å or greater. The angle between the F_{ab} arms is a parameter of great interest. The wide range of possible antigen center-to-center distances for each subclass indicates that the angle between the arms can be small enough for antigen–antigen contact as well as extending to ≈180° for the largest separation distances. The mean angle is 90° based upon a simple trigonometric calculation using a mean separation distance of 130 Å and the geometry defined by the KOL F_{ab_2} crystallographic fragment (Marquart et al., 1980).

Small-angle solution scattering measurements are an average of multiple snapshots of the scattering from different antibody molecules in solution at different times. The structural flexibility observed might therefore be attributed to individual antibody molecules being locked into different conformations for the duration of each 12-h measurement. It seems more likely, however, that each antibody in solution can be found in the full range of accessible conformations over a period of time. In this case, the scattering measurements sample the range of conformations available to each antibody molecule and the variance of the antigen–antigen separation distance is explicitly related to the dynamic flexibility of the F_{ab} subunits. The scattering data, however, contain no information concerning the time scale of the motions.

The flexibility of the F_{ab} subunits is likely to be manifested in a variety of motions. The arms may move independently of each other in an "arm-waving" motion. Other possible motions include a rotation at the hinge region about the long axis of the F_{ab} subunit and a bending motion at the "elbow" joint between the V_H–V_L and the C_H–C_L modules within each F_{ab} subunit (Burton, 1990). Large elbow motions have been questioned by Dangl et al. (1988), who had earlier observed a single decay component in the nanosecond fluorescence anisotropy measurements (Reidler et al., 1982) consistent with a major or single component to the F_{ab} motions. The crystal structures of F_{ab} fragments give widely varying angles for the elbow bends [e.g., 135° in McPC603 (Satow et al., 1986) and 180° in R19.9 (Lascombe et al., 1989)], but these angular changes net only about a 10% change in the distance between the F_{ab} tips.

The high degree of flexibility in the F_{ab}'s might explain the wide variation in the distances between the antigen-binding sites (120–270 Å) determined using a variety of techniques including electron microscopy (EM) and small-angle scattering on a host of different IgG's including human, pig, and rabbit IgG [summarized in Cser et al. (1981b)]. These values are generally larger than one would expect from our scattering data. The average F_{ab} tip-to-tip distance may be slightly smaller than the mean distance between antigen centers (D_c) determined from the neutron-scattering data (117–134 Å) depending on the orientation of the antigen with respect to its binding site. Among the published values, the F_{ab} tip-to-tip distance in closest agreement with our measurements is the 120 Å determined using EM on rabbit IgG (Valentine & Green, 1967). This measurement was based on triangular and quadrilateral formations of IgG molecules for which the angle between the F_{ab} arms is generally much less than 180°. This angle is about 130° in the F_{ab} KOL fragment, which has a tip-to-tip distance of 145 Å (Marquart et al., 1980). The cited values for the F_{ab} tip-to-tip distance in the upper range having an average of 223 Å were generally based upon models derived from small-angle scattering studies which also gave R_g values that were typically 10–40% larger than the value we observed for IgG1 (the only subclass in which aggregation effects could be eliminated). While the 10–40% difference might result from the measurement of antibodies from different species, it may also be due to protein aggregation in the previous works. Finally, the 360 Å value of similar work by Cser et al. (1978) which also used neutron solving matching techniques to measure explicitly the distance between two antibody-bound antigens is significantly larger than that of the current work.

In apparent contrast with our results, nanosecond flourescence experiments by Oi et al. (1984) and Dangl et al. (1988) performed on anti-dansyl murine mAb's indicate that segmental flexibility varies between the IgG subclasses. The degree of flexibility determined by the dansyl rotational correlation times was positively correlated with complement fixation, being greatest for IgG2b, intermediate for IgG2a,

and least for IgG1. The dansyl rotational correlation times, however, are related to the flexibility of both the segmental domains and the entire immunoglobulin. Extracting the F_{ab} motions from the correlation times of the multiple motions of a nonrigid Y-shaped molecule is not currently possible. Thus the primary differences in effector functions of the different subclasses may be related to differences in the relative position and flexibility of F_c (the region known to be responsible for effector functions) with respect to the F_{ab}'s. Flexibility of the F_c region with respect to the F_{ab} arms could, for example, increase the access for binding of the F_c subunit to effector molecules, such as C1, to initiate the classical complement pathway, or to F_c receptors on immune system cells including lymphocytes (Burton, 1990).

The common theme of antibody flexibility is likely to be critical to the molecule's essential purpose: antigen binding. IgG targets antigen either by binding in large numbers to a single antigen or by creating a network of cross-linked antibodies each bound to two different antigens. Flexibility of the hinge region is postulated to increase the ability to form bivalent antigen binding in either of these types of aggregates, and the binding affinity is increased typically by 10^4 for a bivalent antigen (Stryer, 1988). A rigid structure would be less capable of binding bivalently as it could not adapt readily to arbitrary antigen arrangements. One can imagine that bivalent binding begins with binding of the first epitope followed by an "arm-waving" motion that brings the second arm into close proximity to the second epitope. Final docking is potentially achieved through a combination of "elbow-bending" and a rotation about the long axis of the F_{ab} arm.

Registry No. Staphylococcal nuclease, 9013-53-0.

REFERENCES

Alpert, Y., Cser, L., Farago, B., Franek, F., Mezei, F., & Ostanevich, Y. M. (1985) *Biopolymers 24*, 1769.

Alzari, P. M., Lascombe, M.-B., & Poljak, R. J. (1988) *Annu. Rev. Immunol. 6*, 555.

Burton, D. (1990) *Trends Biochem. Sci. 15*, 64.

Cotton, F. A., Hazen, E. E., & Legg, M. J. (1979) *Proc. Natl. Acad. Sci. U.S.A. 76*, 2551.

Cser, L., Gladkikh, I. A., Kozlov, Z. A., Nezlin, R. S., Ogievetskaya, M. M., & Ostanevich, Y. M. (1976) *FEBS Lett. 68*, 283.

Cser, L., Franek, F., Gladkikh, I. A., Nezlin, R. S., Novotny, J., & Ostanevich, Y. M. (1978) *FEBS Lett. 93*, 312.

Cser, L., Franek, F., Gladkikh, I. A., Kunchencko, A. B., & Ostanevich, Y. M. (1981a) *Eur. J. Biochem. 116*, 109.

Cser, L., Gladkikh, I. A., Franek, F., & Ostanevich, Y. M. (1981b) *Colloid Polym. Sci. 259*, 625.

Dangl, J. L., Wensel, T. G., Morrison, S. L., Stryer, L., Herzenberg, L. A., & Oi, V. T. (1988) *EMBO J. 7*, 1989.

Davies, D. R., & Metzger, H. (1983) *Annu. Rev. Immunol. 1*, 87.

Davies, D. R., Padlan, E. A., & Sheriff, S. (1990) *Annu. Rev. Biochem. 59*, 439.

Deisenhofer, J. (1981) *Biochemistry 20*, 2361.

Guinier, A. (1939) *Ann. Phys. (Paris) 12*, 161.

Heidorn, D. B., & Trewhella, J. (1988) *Biochemistry 27*, 909.

Heidorn, D. B., Seeger, P. A., Rokop, S. E., Blumenthal, D. K., Means, A. R., Crespi, H., & Trewhella, J. (1989) *Biochemistry 28*, 6757.

Hjelm, R. P. (1988) *J. Appl. Crystallogr. 21*, 618.

Hubbard, S. R., Hodgson, K. O., & Doniach, S. (1988) *J. Biol. Chem. 263*, 4151.

Kabat, E. A., Wu, T. T., Reid-Miller, M., Perry, H. M., & Gottesman, K. S. (1987) in *Sequences of Proteins of Immunological Interest*, 4th ed., National Institutes of Health, Public Health Service, U.S. Department of Health and Human Services.

Kilar, F., Simon, I., Lakatos, S., Vonderviszt, F., Medgyesi, G. A., & Zavodszky, P. (1985) *Eur. J. Biochem. 147*, 17.

Kringbaum, W. R., & Kugler, F. R. (1970) *Biochemistry 9*, 1216.

Lascombe, M.-B., Alzari, P. M., Boulot, G., Saludjian, P., Tougard, P., Berek, C., Haba, S., Rosen, E. M., Nisonoff, A., & Poljak, R. J. (1989) *Proc. Natl. Acad. Sci. U.S.A. 86*, 607.

Marquart, M., & Deisenhofer, J. (1982) *Immunol. Today 3*, 160.

Marquart, M., Deisenhofer, J., Huber, R., & Palm, W. (1980) *J. Mol. Biol. 141*, 369.

Moore, P. B. (1980) *J. Appl. Crystallogr. 13*, 168.

Noelken, M. E., Nelson, C. A., Buckley, C. E., & Tanford, C. J. (1965) *J. Biol. Chem. 240*, 218.

Oi, V. T., Vuong, T. M., Hardy, R., Reidler, J., Dangl, J., Herzenberg, L. A., & Stryer, L. (1984) *Nature 307*, 136.

Pilz, I., Schwarz, E., & Palm, W. (1977) *Eur. J. Biochem. 75*, 195.

Porod, G. (1982) in *Small Angle X-ray Scattering* (Glatter, O., & Kratky, O., Eds.) pp 33, Academic Press, New York.

Pumphrey, R. (1986) *Immunol. Today 7*, 174.

Rajan, S. S., Ely, K. R., Abola, E. E., Wood, M. K., Colman, P. M., Athay, R. J., & Edmundson, A. B. (1983) *Mol. Immunol. 20*, 787.

Reidler, J., Oi, V. T., Carlsen, W., Minh-Voung, T., Pecht, I., Hersenber, L. A., & Stryer, L. (1982) *J. Mol. Biol. 158*, 739.

Satow, Y., Cohen, G. H., Padlan, E. A., & Davies, D. R. (1986) *J. Mol. Biol. 190*, 593.

Seeger, P. A., Williams, A., & Trewhella, J. (1987) in *Proceedings of the International Collaboration on Advanced Neutron Sources IX* (Atchison, F., & Fischer, W., Eds.) SIN Report ISB 3-907990-01-4, p 437, Swiss Institute for Nuclear Research, Villigen, Switzerland.

Seeger, P. A., Hjelm, R. P., & Nutter, M. J. (1990) *Mol. Cryst. Liq. Cryst. 180A*, 101.

Smith, A. M., Woodward, M. P., Hershey, C. W., Hershey, E. D., & Benjamin, D. C. (1991) *J. Immunol. 146*, 1254.

Stryer, L. (1988) *Biochemistry*, Third ed., pp 894, W. H. Freeman and Company, New York.

Trewhella, J., Carlson, V. A. P., Curtis, E. H., & Heidorn, D. B. (1988) *Biochemistry 27*, 1121.

Valentine, R. C., & Green, N. M. (1967) *J. Mol. Biol. 27*, 615.